J|A|C|S
ARTICLES
Published on Web 04/05/2002

Alkali Metal Intercalated Fullerene-Like MS_2 (M = W, Mo) Nanoparticles and Their Properties

Alla Zak,[†] Yishay Feldman,[‡] Vera Lyakhovitskaya,[†] Gregory Leitus,[†] Ronit Popovitz-Biro,[†] Ellen Wachtel,[‡] Hagai Cohen,[‡] Shimon Reich,[†] and Reshef Tenne*[,†]

Contribution from the Department of Materials and Interfaces, Weizmann Institute, Rehovot 76100, Israel, and Chemical Services Unit, Weizmann Institute, Rehovot 76100, Israel

Received August 28, 2001

Abstract: Layered metal disulfides-MS_2 (M = Mo, W) in the form of fullerene-like nanoparticles and in the form of platelets (crystallites of the 2H polytype) have been intercalated by exposure to alkali metal (potassium and sodium) vapor using a two-zone transport method. The composition of the intercalated systems was established using X-ray energy dispersive spectrometer and X-ray photoelectron spectroscopy (XPS). The alkali metal concentration in the host lattice was found to depend on the kind of sample and the experimental conditions. Furthermore, an inhomogeneity of the intercalated samples was observed. The product consisted of both nonintercalated and intercalated phases. X-ray diffraction analysis and transmission electron microscopy of the samples, which were not exposed to the ambient atmosphere, showed that they suffered little change in their lattice parameters. On the other hand, after exposure to ambient atmosphere, substantial increase in the interplanar spacing (3−5 Å) was observed for the intercalated phases. Insertion of one to two water molecules per intercalated metal atom was suggested as a possible explanation for this large expansion along the *c*-axis. Deintercalation of the hydrated alkali atoms and restacking of the MS_2 layers was observed in all the samples after prolonged exposure to the atmosphere. Electric field induced deintercalation of the alkali metal atoms from the host lattice was also observed by means of the XPS technique. Magnetic moment measurements for all the samples indicate a diamagnetic to paramagnetic transition after intercalation. Measurements of the transport properties reveal a semiconductor to metal transition for the heavily K intercalated 2H-MoS_2. Other samples show several orders of magnitude decrease in resistivity and two- to five-fold decrease in activation energies upon intercalation. These modifications are believed to occur via charge transfer from the alkali metal to the conduction band of the host lattice. Recovery of the pristine compound properties (diamagnetism and semiconductivity) was observed as a result of deintercalation.

Introduction

Transition metal dichalcogenides MS_2 (M = Mo, W) and their intercalated complexes belong to a large class of the so-called two-dimensional or layered solids. The layers of these materials consist of three interconnected, hexagonally arranged, atomic sheets (S-M-S). Trigonal prismatic or octahedral coordination of M to the S atoms occurs within each layer. In MoS_2 and WS_2 variation in the stacking sequence of the layers can lead to the formation of either a hexagonal polymorph with two layers in the unit cell (2H), rhombohedral with three layers (3R), or trigonal with one layer (1T). Atoms within a layer are bound by strong covalent forces, while individual layers are held together by van der Waals (vdW) interactions. The weak interlayer vdW interactions offer the possibility of introducing foreign atoms or molecules between the layers, e.g., via intercalation. By variation of the intercalant and its concentration, a large number of compounds with different properties can be prepared.

A number of experimental methods were used for the metal intercalation into the host MS_2 lattice: (1) immersion of the crystals or powders in metal-ammonia solution or in a solution of butyl-lithium in hexane; (2) exfoliation and subsequent restacking of the suspension of single layer MS_2 around the guest; (3) exposure to metal vapor, and (4) through an electrochemical process. Each method has its pros and cons. In particular, wet (from solution) processes provide very good control of the amount of intercalated atoms, but they usually lead to the co-intercalation of the solvent molecules.

The intercalation mechanism has been elucidated in a number of studies. It has been shown that intercalation of transition metal dichalcogenides by molecules such as ammonia,[1] or alkali atoms[2] develops first by adsorption of the molecules on the outer crystallite surface. Subsequently, a delay period follows, which appears to be associated with the weakening of the vdW forces between the top transition metal dichalcogenide layers. At the

* To whom correspondence should be addressed.
[†] Department of Materials and Interfaces, Weizmann Institute.
[‡] Chemical Services Unit, Weizmann Institute.

(1) (a) Acrivos, J. V. In *Intercalated Layered Materials*; Levi, F., Ed.; D. Reidel Publishing Company: Dordrecht, 1979; Vol. 6, Chapter 1, p 33; b) Beal, A. R.; Acrivos. J. V. *Philos. Mag*. B. **1978**, *37*, 409.
(2) Scrolz, G. A.; Joensen, P.; Reyes, J. M.; Frindt, R. F. *Physica* **1981**, *105B*, 214.

same time, a diffusion of the adsorbed, activated molecules around and in through the edges into these interlayer spaces is followed by weakening of the next layers down and so on. In this way, the elastic energy required to cause the lattice *c*-axis expansion is minimized. An alternative mechanism, where diffusion of the intercalated atoms occurs through the layers was established in the case of Cu on SnS_2[3] and proposed for K on WS_2,[4] both intercalated by exposure to the corresponding metal vapor.

Two main effects were identified as a result of the intercalation: the first − expansion of the interlayer spacing, which can approach 60 Å for organic molecule intercalation complexes;[5] the second − charge transfer from the intercalant to the host material.

Moreover, the tendency for charge transfer from a guest molecule to the host lattice appears to be the driving force for the intercalation reaction. Charge transfer can change the electronic properties of the material, raising the Fermi level, E_F, and increasing the free electron concentration by a few orders of magnitude. Usually, the lowest lying unoccupied energy levels in the host layers are derived from the transition metal d bands. The increase in d band filling of the host material provides the means for a controlled variation of many of its physical properties over a wide range. It is thus possible to achieve semiconductor-to-metal and metal-to-superconductor transitions by intercalation. Thus, semiconducting 2H-MoS_2 intercalated with alkali metals was shown to exhibit metallic behavior and superconductivity with transition temperatures in the range of 3.7 to 6.3 K.[6] Potassium intercalated 2H-WS_2 demonstrates a semiconductor-to-metal transition.[4] The intercalation process can be easily reversed (upon exposure of the sample to air, for example) and the "pure" host compound is recovered. This is an important characteristic for application of these materials as electrodes in secondary (rechargeable) batteries.

The data for lattice expansion and crystallographic transformation in the intercalated complexes is reported and reviewed here in some extent. The immersion of the crystals in alkali metal-ammonia solution for intercalation has been taken first by Rudorff[7] and Somoano et al.[6] resulting in partial intercalation of 2H-MoS_2 with the following stoichiometries: K_xMoS_2 and Na_yMoS_2, $x = 0.4-0.6$ and $y = 0.3-0.6$. X-ray data of the intercalated MoS_2 samples indicated that, the unit cell was expanded upon intercalation, primarily in the *c*- direction. Two different expansions were found by Somoano[6] et al. in sodium and potassium intercalated samples, while only one expansion was found by Rudorff.[7] Thus, K-intercalated materials exhibit the lattice expansion of 4.25 / 5.73 Å[6] or 1.95 Å[7] and Na-intercalated materials 1.59 / 2.65 Å[6] or 1.35 Å.[7] The discrepancy between the lattice parameters of the same system, observed in the different works, can be probably attributed to the insertion of ammonia molecules (solvent) or water uptake from the environment by the intercalated metal atoms during or shortly after the process.

The water uptake (hydration) by intercalated alkali metals was discussed in detail by Wypych et al.[8−10]The alkali metal intercalated materials were found to undergo hydration and partial oxidation by washing with water to form $K_{1-x}(H_2O)_yMoS_2$. It was shown that the spacing along the *c*-axis of the intercalated crystals varies during the hydration reaction.

The K- and Na-intercalation of MS_2 (M = Mo, W) by the exfoliation/restacking technique resulted in interlamellar *d* spacing in the range of 9.3−9.7 Å (Δc / 2 = 3.1−3.5 Å expansion), which was attributed to co-intercalation of approximately one monolayer of water molecules.[11] 2H−MoS_2 intercalated with Mn, Fe, Co, and Ni by the same technique reveals interlayer spacing expansion (Δc / 2) in the range of 5.1−5.3 Å**,** which is attributed to the co-intercalation of the metal atom together with two layers of water molecules.[12,13] Solid-state NMR study of the hydrated alkali-metal intercalated compounds of MoS_2 indicates on similar different expansions due to the different degree of hydration.[14]

Py et al.,[15] who have used the butyl-lithium technique for the metal intercalation, show that in addition to lattice expansion, the structure of 2H-MS_2 may partially distort to 1T-MS_2 upon intercalation. Later on, it was reported[16] that for low Li content ($x = 0.35$ in Li_xWS_2) the diffraction pattern was identical to that of 2H−WS_2, with no change in basal plane spacing. However, for high lithium content ($x > 1$), the diffraction pattern shows a crystallographic transformation, where the transition metal coordination changes from trigonal prismatic (2H) to octahedral (1T). For moderate Li content ($x = 0.8$), a mixed phase of 2H and 1T was observed. At the same time, the *c*-lattice constant expands. Moreover, the 1T polytype has a metallic character. However, the distorted 1T-MS_2 phase is known to be metastable and transforms to the thermodynamically stable 2H-MoS_2 upon heating (above 90 °C) or aging in air, and simultaneously the guest species are reduced and deintercalated.[13] Different structures also were found, depending on the thermal history of each sample.

Some intercalation compounds (graphite, for example)[5,17−19] exhibit a high degree of ordering, which is revealed in a staging phenomenon. Ordering of the guest atoms (staging) in intercalation complexes of transition metal dichalcogenides has been observed only with certain concentrations of intercalant atoms and at low temperatures (Ag in TiS_2, for example).[17]

Nanoparticles of layered compounds (graphite, transition metal dichalcogenide, BN, $NiCl_2$, etc.) were shown to be unstable against folding and they close into fullerenes or fullerene-related structures (single or multiwall polyhedra, and

(3) (a) Ohuchi, F. S.; Jaegermann, W.; Parkinson, B. A. *Surf. Sci.* **1988**, *194*, L69; b) Jaegermann, W.; Ohuchi, F. S.; Parkinson, B. A. *SIA Surf. Interface Anal.* **1988**, *12*, 293.
(4) Ohuchi, F. S.; Jaegermann, W.; Pettenkofer, C.; Parkinson, B. A. *J. Am. Chem. Soc.* **1989**, *5*, 439.
(5) Liang, W. Y. In *Intercalation in Layered Materials*; Dresselhaus, M. S., Ed.; NATO ASI Series B: Physics, Plenum Press: New York, 1986; Vol. 148, p 31.
(6) Somoano, R. B.; Hadek, V.; Rembaum, A. *J. Chem. Phys*. **1973**, *58*, 697.
(7) Rudorff W. *Chimia* **1965**, *19*, 489.
(8) Wypych, F.; Schollhorn, R. *J. Chem. Soc., Chem. Commun.* **1992**, 1386.
(9) Wypych, F.; Weber, Th.; Prins, R. *Surf. Sci.* **1997**, *380*, L474-L478.
(10) Wypych, F.; Solenthaler, C.; Prins, R.; Weber, Th. *J. Solid State Chem.* **1999**, *144*, 430.
(11) Heising, J.; Kanatzidis, M. G. *J. Am. Chem. Soc.* **1999**, *121*, 11720.
(12) Zubavichus, Y. V.; Slovokhotov, Y. L.; Schilling, P. J.; Tittsworth, R. C.; Golub, A. S.; Protzenko, G. A.; Novikov, Y. N. *Inorganica Chimica Acta* **1998**, *280*, 211.
(13) Dungey, K. E.; Curtis, M. D.; Penner-Hahn, J. E. *Chem. Mater*. **1998**, *10*, 2152.
(14) Alexiev, V., Meyer, H. zu Altenschildesche, Prins, R., Weber, Th. *Chem. Mater.* **1999**, *11*, 1. 1742−1746..
(15) Py, M. A.; Haering, R. R. *Can. J. Phys.* **1983**, *61*, 76.
(16) Yang, D.; Frindt, R. F. *J. Phys. Chem. Solids* **1996**, *57(6−8)*, 1113−1116.
(17) Brec, R. and Rouxel, J.; Brec, R. In *Intercalation in Layered Materials*; Dresselhaus, M. S., Ed.; NATO ASI Series B: Physics, Plenum Press: New York, 1986; Vol. 148, 31−125.

nanotubes).[20−24] In analogy to their macroscopic counterparts, it is expected that the structural as well as the electrical and magnetic properties of these nanoparticles could be modified as a result of intercalation with various species.

Thus, intercalation of multiwall carbon nanotubes with alkali metal atoms from the vapor phase was recently described.[25] The intercalated nanotubes were found to be arranged in a stage-1 superlattice, i.e., alkali metal layers were stacked between each two carbon layers. Electrochemical intercalation of lithium into multiwall carbon nanotubes reveals heterogeneous swelling of the tubes, and this process was found to be reversible.[26] Similar structures were observed in K- and $FeCl_3$- intercalated carbon nanotubes, obtained through a gas-phase reaction.[27] Here, the intershell spacing increases significantly from 3.44 to 5.3 Å as a result of K intercalation and nearly triples as a result of $FeCl_3$ intercalation, up to the value of 9.5 Å. The composite nanostructures were found to disintegrate when exposed to air, and complete shattering of the nanotubes occurred upon immersion in water.

Sodium intercalated fullerene-like WS_2 material was obtained by doping of an oxide precursor, and subsequent sulfidization of the oxide nanoparticles.[28] The intercalated moieties afforded staging ($n = 6$) and were found to be stable in air and even in ethanol.

In the present work, inorganic fullerene-like (*IF*) nanoparticles (*IF*-MS_2, M = Mo, W) were intercalated by exposure to alkali metals' (sodium and potassium) vapor. Synthesis of macroscopic quantities of a pure *IF*-MS_2 phase[29−31] provided sufficient material to carry out these experiments. For the sake of comparison, molybdenum/tungsten disulfide powders in the form of 2H-MS_2 platelets were also intercalated under similar conditions. Chemical analysis of *IF*-MS_2 nanoparticles and 2H-MS_2 platelets before and after intercalation is presented. Intercalated *IF* and 2H materials exhibit substantial increase in the interplanar spacing (3−5 Å), which was attributed to the insertion of one to two water molecules per intercalated metal atom. High temperature preparation of the intercalated materials excluded the formation of the thermally unstable 1T-phase of the product. X-ray intensity data were used to estimate the portion of the sample actually intercalated. The transport and magnetic properties of the intercalated samples changed significantly under intercalation and these data are presented.

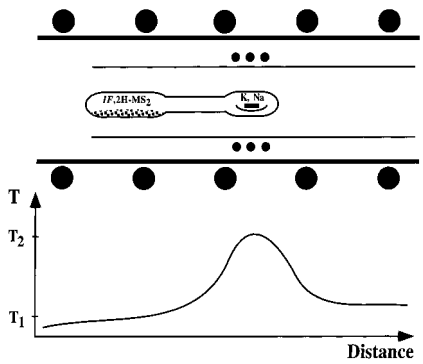

Figure 1. Illustration of the experimental setup used for the intercalation.

Experimental Section

Starting materials of four different kinds were studied in this work. The *IF*-MS_2 nanoparticles were obtained by high-temperature sulfidization of the respective trioxide powders in a reducing atmosphere.[29−31] The *IF*-MoS_2 nanoparticles were 0.005−0.3 μm in diameter, with 0.1-μm size dominant. The *IF*-WS_2 nanoparticles were 0.1−0.3 μm in diameter, with 0.2-μm size dominant. 2H-MoS_2 (99%) and 2H-WS_2 (99.8%) powder in the form of 3.0−5.0 μm platelets were purchased from Alfa Aesar and used as received.

Alkali metals − sodium and potassium − were used as intercalants. A two-zone vapor transport technique was applied for the present study. Pure K (Na) metals and powders of 2H-MS_2 or *IF*-MS_2 were loaded in two-section Pyrex/quartz ampules to secure the spatial separation of the host material and the intercalating solid. The alkali metal was placed into a tungsten container to prevent its reaction with the glass. The ampules were sealed off under vacuum (10^{-5} Torr), after 2−3 h of evacuation, and placed in a horizontal two-zone furnace. To achieve a temperature gradient, an additional 2.5-cm length furnace was inserted (see Figure 1).

For the intercalation process, the temperature of the starting materials (T_1) was varied from 100 to 500 °C, while the temperature for the intercalant (T_2) was 20−30 °C higher than T_1. To prevent condensation of the metal on the sample, an opposite gradient ($T_1 > T_2$) was applied during sample cooling. The intercalation period was varied from 2 to 24 days.

Unfortunately, a pure phase of intercalated material could not be obtained in either case (see below). No attempt was made to separate the intercalated product from the nonintercalated phase. Intercalation of a larger amount of the alkali metal in the host phases resulted in a deposition of the alkali metal on the particles' surface. Such samples are pyrophoric in the ambient atmosphere. Alternatively, if the excess of alkali metal was not substantial, the samples were very hygroscopic.

All the operations with alkali metals, as well as with the intercalated samples, were processed in a glovebox under argon atmosphere. Special care was undertaken to minimize the exposure of the intercalated samples to the ambient atmosphere during transfer to the various analyses.

A X-ray powder diffractometer (XRD), Rigaku D/MAX-B with graphite monochromatized CuKα radiation (1.54178 Å), was used to analyze the materials. The powders were affixed to glass slides (1.5 cm^2) via double-sided tape and measured in

(18) Dresselhaus, M. S.; Dresselhaus, G. *Adv. Phys.* **1981**, *30*, 139−326.
(19) Fisher, J. E In *Intercalated Layered Materials*; Levi, F., Ed.; D. Reidel Publishing Company: Dordrecht, 1979; Vol. 6, Chapter 2, p 481;
(20) Kroto. H. W.; Heath, J. R.; O'Brien, S. C.; Curl, R. F.; Smalley, R. E. *Nature* **1985**, *318*, 162.
(21) Iijima, S. *Nature* **1991**, *354*, 56.
(22) (a) Tenne, R.; Margulis, L.; Genut, M.; Hodes, G. *Nature* **1992**, *360*, 444; b) Margulis, L.; Salitra, G.; Tenne, R.; Talianker, M. *Nature* **1993**, *365*, 113.
(23) (a) Stephane, O.; Ajayan, P. M.; Colliex, C.; Redlich, Ph.; Lambert, J. M.; Rernier, P.; Lefin, P. *Science* **1994**, *226*, 1683; b) Chopra, N. G.; Luyken, J.; Cherry, K.; Crespi, V. H.; Cohen, M. L.; Louie, S. G.; Zettl, A. *Science* **1995**, *269*, 966.
(24) Rosenfeld Hacohen, Y.; Grunbaum, E.; Tenne, R.; Sloan, J.; Hutchison, J. L. *Nature* **1998**, *395*, 336.
(25) Zhou, O.; Fleming, R. M.; Murphy, D. W.; Chen, C. H.; Haddon, R. C.; Ramirez, A. P.; Glarum, S. H. *Science* **1994**, *263*, 1744.
(26) Maurin, G.; Bousquet, Ch.; Henn, F.; Bernier, P.; Almairac, R.; Simon, B. *Chem. Phys. Lett.* **1999**, *312*, 14.
(27) Mordkovich, S.; Baxendale, S.; Yoshimira, S.; Chang, R. P. H. *Carbon* **1996**, *34*, 1301.
(28) Homyonfer, M.; Alperson, B.; Rosenberg, Y.; Sapir, L.; Cohen, S. R.; Hodes, G.; Tenne, R. *J. Am. Chem. Soc.* **1997**, *119*, 2693.
(29) Feldman, Y.; Frey, G. L.; Homyonfer, M.; Lyakhovitskaya, V.; Margulis, L.; Cohen, H.; Hodes, G.; Hutchison, J. L.; Tenne, R. *J. Am. Chem. Soc.* **1996**, *118*, 5362.
(30) Feldman, Y.; Zak, A.; Popovitz-Biro, R.; Tenne, R. *Solid State Sciences* **2000**, *2*, 663.
(31) Zak, A.;Feldman, Y.; Alperovich, V.; Rosentsveig, R.; Tenne, R. *J. Am. Chem. Soc.* **2000**, *122*, 11108.

the open air under a N_2 stream. Nevertheless, reaction with water could not be fully prevented in these experiments during the scan (20 min). XRD measurements of samples covered by a protective X-ray transparent Kapton film were also carried out. However, the signal-to-noise ratio was fairly low in this case and furthermore, no perfectly hermetic water-isolation was achieved.

More rigorous elimination of the ambient atmosphere could be accomplished using a flat plate wide-angle X-ray scattering (WAXS) setup, in which the material was confined in glass/quartz capillaries, sealed in the glovebox. In this setup, a Searle camera with Franks optics affixed to an Elliott GX6 rotating anode generator was used. The patterns were obtained in transmission mode on imaging plates (Fuji), which were scanned with a He−Ne laser (Spectra Physics) in conjunction with a homemade reader based on an Optronics (Chelmsford, USA) densitometer and interfaced to a PC. Images were processed using the public domain ImageJ program. Only a few samples were studied using this technique. Fresh samples and samples stored in air for different periods of time were analyzed by both XRD and WAXS.

Transmission electron microscopy (TEM), performed on Philips model CM-120, was used for the characterization of the samples before and after intercalation. A procedure for the transfer of samples to the TEM with (almost) no exposure to the atmosphere was found to be of key importance for the present study.

The chemical composition of the investigated materials was determined by X-ray energy dispersive spectrometers (EDS), Link model ISIS, mounted on the scanning electron microscope (SEM), JEOL 6400 and EDAX mounted on the TEM. Whereas the depth/area probed by the EDS/TEM is in the range of 50 nm / 2500 nm^2, the depth/area probed by the EDS/SEM setup is typically 1 μm / 1 μm^2. Therefore, the former can in principle analyze a single nanoparticle, while the latter can only probe a group of nanoparticles. Also note that this technique is unable to detect concentrations of the intercalant of less than about 0.5 atomic percent (at. %).

X-ray photoelectron spectroscopy (XPS) was carried out using the Kratos AXIS−HS instrument with a low power (75 W) monochromatized Al (Kα) source. The samples were transferred from the glovebox into the chamber under vacuum conditions. The analysis depth/area was ca. 5 nm / 1 mm^2. A flood gun was used for the variation of the surface charging conditions, where the electron kinetic energy ranged between 2 and 4.5 eV.

Magnetic susceptibility as well as resistivity measurements were taken with a commercial SQUID magnetometer (MPMS-2 of Quantum Design), operating at an applied magnetic field of 0.01−0.05 T and in the temperature range from 2 to 300 K. For the magnetic measurements, the samples were charged into calibrated gelatin capsules in an inert atmosphere glovebox and fixed to the end of the sample rod.

For the resistivity measurements, pellets 3 mm in diameter and ca. 1 mm thick were prepared from pristine and intercalated powders under 0.5-ton force press. Contacts to the samples were established under a microscope in the ambient atmosphere. Finally, thin gold wires, 0.1-mm thick, were glued by silver paint (0.01 Ω*cm) to the sample and to the contacts of the substrate to establish the electrical connection between sample and apparatus. These contacts normally proved to be of sufficient quality to enable accurate resistivity measurements. The measurements were carried out in the van der Pauw configuration,[32] suitable for flat samples of arbitrary shape with sufficiently small contacts located at the circumference of the sample. Both magnetic and transport measurements were done for the impure material, which consists of a mixture of intercalated and nonintercalated powders.

Results and Discussion

1. X-ray Diffraction. *1a. WAXS Measurements.* WAXS measurements were carried out for K-intercalated *IF*-WS_2 samples, which were hermetically sealed in capillaries under inert (Ar) atmosphere. In this technique, concentric rings represent diffraction from individual crystallographic planes (see Figure 2). Figure 2a shows the pattern of pristine *IF*-WS_2. The (002), (004), (101), and (100) diffraction rings are clearly observed in this figure. Figure 2b has been obtained from a freshly intercalated sample, and it contains essentially the same diffraction rings as the pristine sample. To our experimental resolution, no shift or broadening of the (002) ring can be detected. This result can be due to the random distribution of guest atoms inside the layers and the relatively small concentration of the intercalant in the host material ($\approx$ 10 at. % on average, which is equivalent to $K_{0.3}WS_2$), and is in agreement with a previous report.[15]

Figures 2c and 2d were obtained after exposure of the sample to the ambient atmosphere for three days and six days, respectively. Most strikingly, additional diffraction rings were revealed in the pattern after three days exposure to the ambient atmosphere (Figure 2c). These changes are believed to arise from the swelling of the lattice due to hydration of the alkali atoms inside the *IF* lattice. This process leads to the formation of new lattices with different lattice constants in the *c*-direction. Taking into account the high temperature preparation of the intercalated materials, formation of the thermally unstable 1T-phase of the product was excluded. Thus, the new rings can be ascribed to the $(00l)'$ series of reflections, which can be identified as $(002)_1'$ with $c/2 = 8.38$ Å, $(002)_2'$ with $c/2 = 9.81$ Å and $(002)_3'$ with $c/2 = 11.32$ Å, and their second-order reflections (see Figure 2c). Some reflections could not be identified, however. Larger *d* spacing, corresponding to rings with smaller radii, can be attributed to (001) reflections, which are forbidden but can appear in distorted structures.

After six days in the ambient atmosphere some of the $(00l)'$ rings disappear (Figure 2d), while the intensity of the $(002)_2'$ with $c/2 = 9.81$ Å becomes almost as strong as that of the unaltered (002) ring. In accordance with previous reports[11,14,33], such an expansion can be explained by co-encapsulation of approximately one monolayer of water. XRD data for K-intercalated *IF*-WS_2, which is shown below, reveals the same lattice expansion. After one month in the ambient atmosphere, the diffraction pattern (not shown) assumes a form very close to that of Figure 2b, indicating a deintercalation process.

1b. Powder Diffraction (XRD). Here measurements were done in the open air under a N_2 gas stream. Therefore, the influence of the ambient humidity was observed during the X-ray scan (20 min).

(32) Pauw, L. J. *Philips Res. Repts.* **1958**, *13*, 1−9.

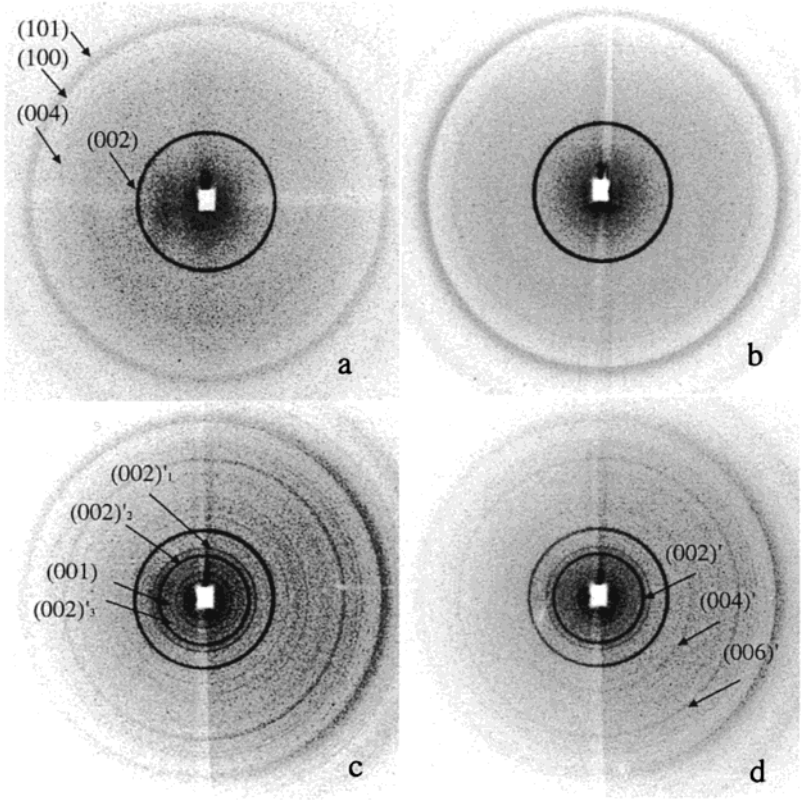

Figure 2. Wide-angle X-ray scattering (WAXS) patterns: (a) pristine *IF*-WS_2; (b) freshly K-intercalated *IF*-WS_2 nanoparticles; (c) after exposure of sample-b to the ambient atmosphere for three days; (d) after a six-day exposure of sample-b to the ambient atmosphere.

All four kinds of precursors, 2H-MS_2 and *IF*-MS_2 (M = Mo, W), intercalated by both K and Na were characterized by XRD. However, only two X-ray patterns, each of them typical for one kind of intercalant are discussed in detail in the present report. A more detailed account of these measurements will appear elsewhere.

The XRD pattern of pristine *IF*-WS_2 nanoparticles 100−300 nm in diameter is shown in Figure 3A(a). In accordance with previous studies,[34] the (00*l*) peaks of the pristine fullerene-like phase is shifted toward lower angles, indicating expansion of the lattice along the *c*-axis, in comparison with the 2H-phase (vertical line). This shift is attributed to the strain release mechanism in these folded structures. Figures 3A(b-d) show the XRD patterns for *IF*-WS_2 after intercalation with K. Figure 3A(b) has been obtained for a fresh sample, while Figures 3A-(c) and 3A(d) were obtained after exposure of the sample to the ambient atmosphere for one month and six months, respectively. Similar patterns were obtained for all types of precursors after K-intercalation.

The diffraction pattern of the fresh sample (Figure 3A(b)) shows Bragg peaks of the pristine *IF* nanoparticles as well as a new set of reflections. The XRD spectrum of the intercalated phase can be indexed on the basis of the hexagonal (2H) unit cell with $a = 3.18$ Å and $c = 18.96$ Å. Therefore, the spacing between two adjacent layers in the expanded lattice of the intercalated phase is $c / 2 = 9.48$ Å. The corresponding spacing of the nonintercalated phase is $c_0 / 2 = 6.26$ Å. Therefore, the increase in the interlayer distance as a result of the intercalation is $\Delta c / 2 = (c - c_0) / 2 = 3.22$ Å. Based on the foregoing discussion of the WAXS measurements and the TEM analysis (vide infra), which were done under careful exclusion of humidity, it can be concluded that the new series of peaks (00*l*)′ emanate from the interaction of the sample with the ambient atmosphere during the measurement. In particular, this series of diffraction peaks reflect the hydration of the intercalated ions, which leads to significant lattice expansion and to a new crystalline order within the particles. Substantial water intercalation during the short period of XRD scan of the fresh sample may have occurred due to X-ray assisted chemical changes in the specimen.

XRD measurements of the freshly K-intercalated *IF*-WS_2 samples were also carried out under protective Kapton film. A smaller lattice expansion ($\Delta c / 2 = 2.74$ Å) was observed in this case, which shifted to the previous value (3.22 Å) when the Kapton film was removed. These results indicated again some water intercalation under the protective film, which does not lead to a perfectly hermetic sealing.

The exposure of the freshly K-intercalated *IF*-WS_2 samples to the ambient atmosphere for prolonged periods of time results in changes in the XRD pattern, similar to those observed by WAXS. Figure 3A(c) shows that after one month storage in air the intensity of (002)′ and (004)′ peaks is reduced and both reflections are shifted toward smaller angles ($c / 2 = 9.72$ Å or $\Delta c / 2 = 3.46$ Å). This additional shift is ascribed to the continuous K−H_2O interaction, which leads to further water intercalation into the vdW gap between two WS_2 layers, and consequently further lattice expansion. The reduction in the (002)′ peak intensity is associated with slow deintercalation of the hydrated potassium ions. Figure 3A(d) corresponds to the

(33) Wells, A. F.; *Structural Inorganic Chemistry*; Oxford University Press Inc.: New York, 5th ed., 758.
(34) Feldman, Y.; Wasserman, E.; Srolovitz, D. J.; Tenne, R. *Science* **1995**, *267*, 222.

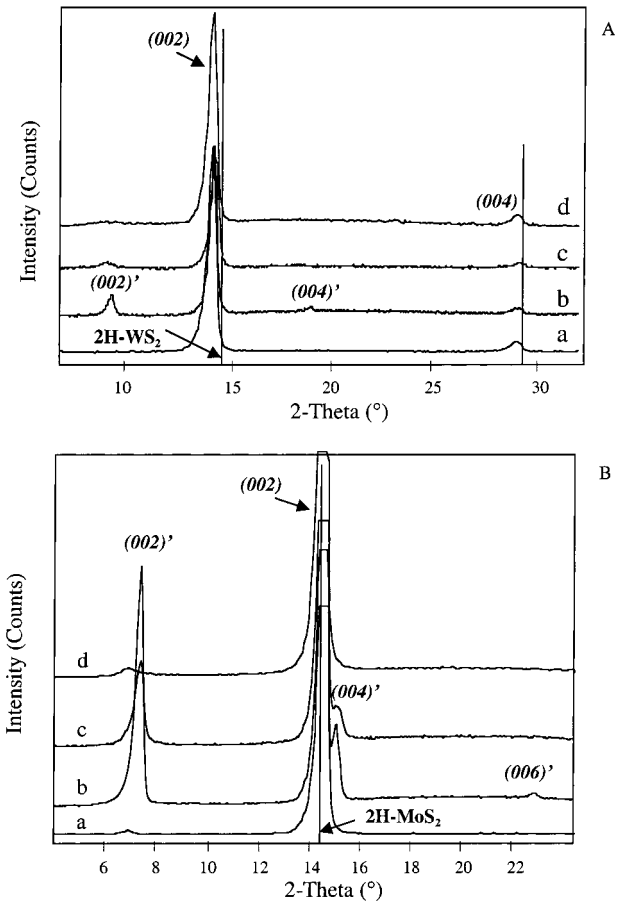

Figure 3. A. X-ray diffraction patterns: (a) pristine *IF*-WS_2; (b) freshly K-intercalated *IF*-WS_2 nanoparticles; (c) after exposure of sample-b to the ambient atmosphere for one month; (d) after a six-month exposure of sample-b to the ambient atmosphere (deintercalated sample). B. X-ray diffraction patterns for sample I of 2H−MoS_2: (a) pristine 2H−MoS_2; (b) freshly Na-intercalated MoS_2 platelets; (c) after exposure of sample-b to the ambient atmosphere for two weeks; (d) after 6 month exposure of sample-b to the ambient atmosphere (deintercalated sample).

XRD pattern after half a year exposure to the ambient atmosphere, which is rather similar to the XRD pattern of the original material (compare with Figure 3A(a)). Therefore, when the intercalated sample is exposed to the ambient atmosphere, first water insertion into the host lattice and partial hydration of the alkali ions takes place. Longer exposure to the ambient atmosphere leads to further water occlusion into the vdW gap. The fully hydrated alkali ions (single water layer) leach out of the covalent host lattice leading thereby to restacking of the MS_2 layers. These observations lead to the conclusion that the intercalation process in fullerene-like materials is reversible, in agreement with the WAXS results.

The XRD pattern of K-intercalated 2H- and *IF*-WS_2 after two years storage in a glovebox (argon atmosphere) revealed a very small reduction in the (00*l*)′ peaks intensity and a negligible shift toward higher *d* spacing in comparison with fresh samples. This finding suggests that the intercalated phase with alkali atoms is relatively stable under inert atmosphere.

Figure 3B shows the X-ray patterns for sample I of 2H−MoS_2 before (Figure 3B(a)) and after intercalation (Figures 3B-(b-d)) with Na. Here too, the diffraction pattern clearly reveals that the treated fresh sample consists of a mixture of nonintercalated and intercalated phases (Figure 3A(b)), and water intercalation occurs during the XRD measurements of the fresh

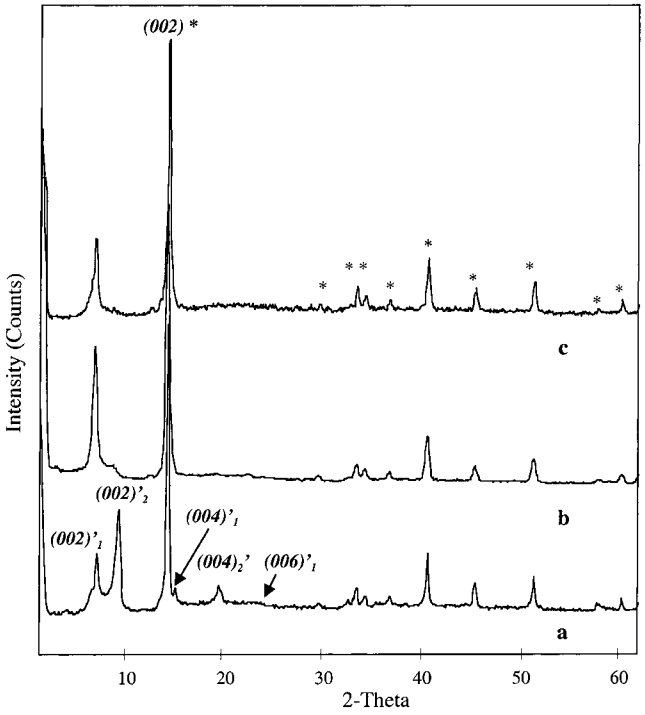

Figure 4. X-ray diffraction patterns for sample II of 2H−MoS_2: (a) freshly Na-intercalated MoS_2 platelets; (b) after exposure of sample-a to the ambient atmosphere for two weeks; (c) after one-month exposure of sample-a to the ambient atmosphere. All the reflections, which belong to the XRD pattern of the nonintercalated phase, are denoted by (*).

sample. Three extra peaks, which were indexed as the (002)′, (004)′, and (006)′ reflections are assigned to an expanded 2H unit cell with $c / 2 = 11.94$ Å as compared with $c_0 / 2 = 6.15$ Å for the pristine phase. The larger lattice expansion ($\Delta c / 2 = 5.66$ Å) in this case is likely to stem from a stronger Na-water interaction, as compared to the case of K.[35] This result is also in a good agreement with the literature[12−14,33], where the interlayer spacing of MS_2 was increased to ≈ 9 or 12 Å by a single or double layer of hydrated K^+ or Na^+, as well as other ions.

Prolonged (two weeks) storage of the Na intercalated 2H−MoS_2 sample in air leads to a substantial reduction in the intensity of the (00*l*)′ diffraction peaks (Figure 3B(c)). At the same time the intensity of the (00*l*) peaks, corresponding to the nonintercalated phase in this sample, increased (not shown). Storage of the sample in the ambient atmosphere for about half a year led to a complete disappearance of the (00*l*)′ peaks (Figure 3B(d)), i.e., Na atoms were dissolved by the water molecules and leached out of the host lattice.

Depending on experimental conditions some of the Na intercalated 2H-MS_2 samples may reveal two additional series of (00*l*)′ peaks (Figure 4). For sample II of 2H−MoS_2 the $(002)_1$′ and $(002)_2$′ peaks corresponds to lattice spacing of 9.5 and 11.5 Å ($\Delta c / 2 = 3.2$ and 5.2 Å). Furthermore, after storage in ambient conditions, the peaks of the lower d-values moved to the higher ones until they merged together and later on, gradually disappeared. This observation suggests that initially the Na atoms adsorb only a single hydration layer, while a second hydration shell is slowly introduced into the host lattice at a

(35) Cotton, A. F.; Wiikinson, G.; Murillo, C. A.; Bochmann, M.; *Advanced Inorganic Chemistry*; 6th ed.; John Wiley & Sons, Inc.: New York, 1999; p 102.

Table 1. Volume Fraction (V_K,%) of the Intercalated Phase, Alkali-metal/Transition-metal Atomic Ratio (K:Mo) and Atomic Concentration (at. %) of K in the Host Lattice.[a]

K-intercalated Materials	c_o, Å[b]	c, Å[c]	$\Delta c/2$, Å[d]	VK, %	K:Mo (atomic ratio)	at. % of K
2H-MoS_2	12.29	18.42	3.07	13.6	1:10.6	3.05
IF-MoS_2	12.54	18.63	3.05	11.6	1:10.9	2.97
2H-WS_2	12.36	18.54	3.09	13.4	1:8	4.00
IF-WS_2	12.52	18.96	2.98	13.1	1:8.5	3.79

[a] Data were Calculated using the experimental powder XRD data (c, c_0) for the K-intercalated and nonintercalated phase. [b] c_0 -is a lattice constant of pristine/nonintercalated powders. [c] c -is a lattice constant of intercalated one. [d] $\Delta c / 2 = (c - c_0)/2$ is the expansion of the interlayer spacing as a result of intercalation.

Table 2. Potassium and Sodium Atomic Concentration (at. %) in Intercalated 2H-MS_2 and *IF*-MS_2 Obtained from EDS/SEM Analysis

	+ K		+ Na	
samples	at. %	K:M (atomic ratio)	at. %	Na:M (atomic ratio)
2H-MoS_2	8−18	1:4 − 1:1.5	2−11	1:16 − 1:2.7
IF-MoS_2	2−7	1:16 − 1:4.4	2−6	1:16 − 1:5.2
2H-WS_2	2−12	1:16 − 1:2.4	2−10	1:16 − 1:3
IF-WS_2	2−10	1:16 − 1:3	2−8	1:16 − 1:3.8

later stage. Finally, the alkali atoms are dissolved by the adsorbed water molecules and are extracted from the host lattice. The rate of alkali metal deintercalation was found to be 50−100% faster for the intercalated 2H phase as compared to the *IF* phase.

Note that the *IF*- phase usually reveals only the smallest lattice spacing, i.e., $\Delta c / 2 \approx 3.2$ Å, for both K and Na intercalation. This observation suggests that the alkali metal atoms accommodate only one hydration layer in the seamless structure of the *IF* nanoparticles.

It is clear from the XRD analysis that the intercalated product consists of a mixture of nonintercalated and intercalated phases, while the intercalated phase is arranged in a stage 1 superlattice (i.e. hydrated alkali metal layers stacked between each two S-M-S layers) and the nonintercalated phase remains in the pristine form. Moreover, the two phases can coexist on the same 2H-platelet or *IF*-nanoparticle, which will be demonstrated in the TEM section (vide infra). These materials did not exhibit any staging other than $n = 1$, which is in agreement with previous report.[7]

An attempt to estimate the volume fraction (%) occupied by the intercalated phase ($V_K = (V_{KMoS2} / (V_{KMoS2} + V_{MoS2}))*100$) was done from the experimental and theoretical relative intensities of the XRD $(00l)'$ reflections of both the pure and the intercalated phases (see Table 2). Theoretical XRD intensities were calculated using the "LAZY PULVERIX" program[36] and the following model for the intercalated phase. The intercalating alkali atoms were placed in the octahedral sites within the vdW gap of the expanded unit cell, and a full occupancy of these sites, i.e., K:Mo = 1:1 **(**$KMoS_2$**)** was assumed for the intercalated phase.[37] The *c*-axis parameters of the intercalated unit cells were taken from the experimental X-ray diffraction patterns and are presented in Table 2. K:Mo average atomic ratio ($N_K / (N_K + N_{Mo})$) as well as atomic percent (at. %) of K in the powders after intercalation was calculated from the V_K data and the volume occupied by the unit cell of each phase (Table 1). As it is readily apparent from Table 2, the volume fraction of intercalated phase constitutes 11−13% of the starting material, which is 3−4 at. % of the alkali metal on average.

2. Energy-Dispersive X-ray analysis (EDS). The average chemical composition of the intercalated materials was determined by EDS in SEM analysis. The data were collected from five to ten different locations on each sample and are presented as at. % considering K, Mo(W), and S as 100%.

The atomic concentration of potassium in the intercalated 2H−MoS_2 as a function of the reaction time and temperature was studied. It was found that the atomic concentration of the intercalant depends on the duration and temperature regime of the intercalation. The highest K content − 8−18 at. % was obtained after 12 days annealing at $T_1 / T_2 = 290 / 320$ (°C). This regime was applied for the potassium intercalation of all the materials studied. Further prolongation of the intercalation period did not lead to a higher K content. An additional increase of the intercalation temperature reveals a decreasing amount of the intercalant population. The time and temperature dependence of the intercalant uptake suggests that the process of intercalation is a diffusion controlled process.

The optimal temperature regime for the Na-intercalation process was found to be $T_1 / T_2 = 410 / 435$ °C. It is worth noting that a similar vapor pressure of $\approx 10^{-1}$ Torr is attained for K at $T_2 = 320$ °C and for Na at $T_2 = 435$ °C. The results of the EDS / SEM analysis for different samples intercalated with K and Na in the optimal intercalation regimes are summarized in Table 2. Scatter of the data was observed in all EDS measurements as a result of sample inhomogeneity.

It is clear from the data shown in Table 2, that the atomic concentration of the intercalant that could be taken-up by the fullerene-like nanoparticles was usually smaller than that of the bulk 2H phase. In the case of the platelets, facile intercalation through the prismatic face ($\{hk0\}$) is possible. In the case of *IF* nanoparticles, the guest atoms must diffuse through the closely packed atoms in the $a - b$ ($<00l>$ direction) plane, or through point defects or grain boundaries. Furthermore, the intercalation of guest atoms between two closed atomic cages bears a large penalty in elastic energy. This extra strain increases with shrinking *IF* radius and the number of *IF* intercalated layers. For the same reasons, the deintercalation process was found to be faster for the 2H-WS_2 (and 2H-MoS_2), than that for the respective *IF* phase.

The data in Tables 1 and 2 that might appear at first glance to be incompatible with each other, actually represent different analyses. The XRD measurements were taken from a large sample volume. Consequently, the K:Mo ratio obtained by this method reflects a sample average. On the other hand, the EDS/SEM analysis was made on a small group of intercalated nanoparticles. The discrepancy between the low values of the atomic concentrations of the intercalated alkali metals, obtained from the XRD data, and the much higher values obtained by EDS, reflect also the possible idealization of the model used for fitting the XRD data.

3. TEM Analysis. The structure of the pristine and intercalated fullerene-like nanomaterials with typical spherical and polyhedral shapes were investigated.

(36) *http://crystsun1.unige.ch/ilicrx/lazy.html.*
(37) Water molecules were disregarded in the present calculations, since their scattering intenstiy is very weak compared with the W (Mo) atoms.

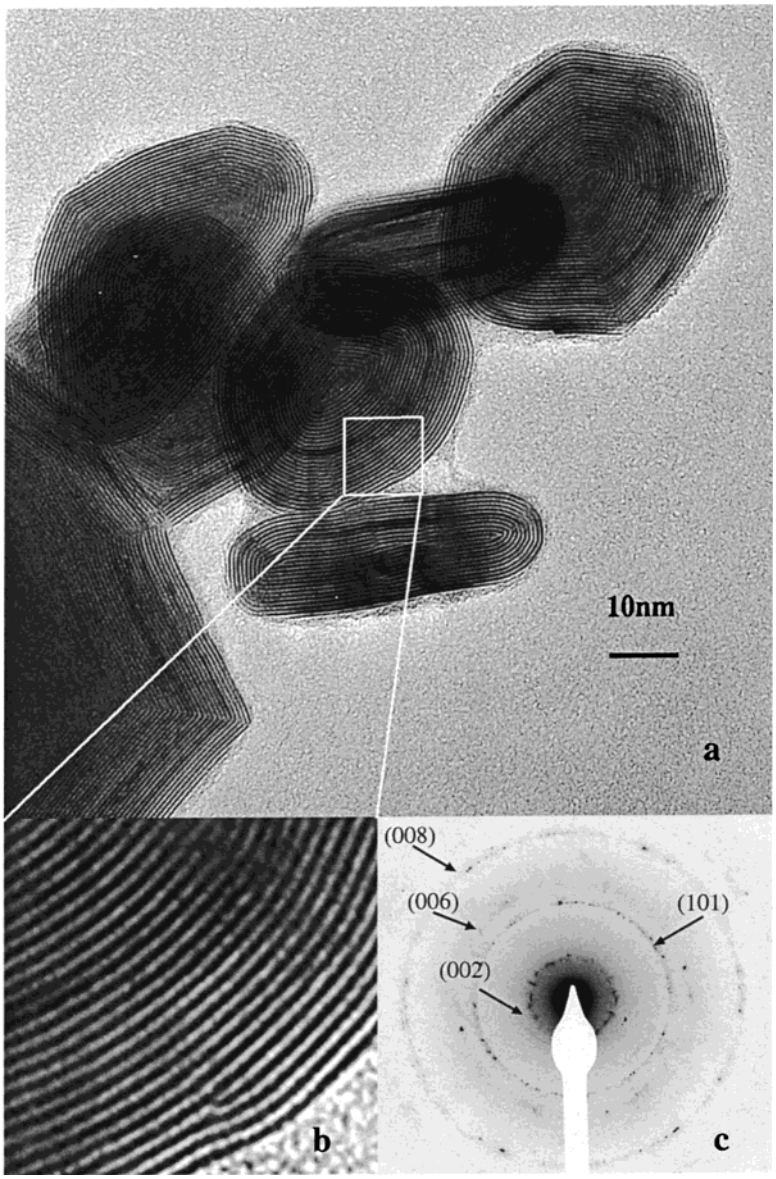

Figure 5. (a) TEM micrograph of pristine *IF*-MoS_2 nanoparticles; (b) exploded view of the frame; (c) electron diffraction of (a).

TEM images of *IF*-MoS_2 nanoparticles before and after intercalation are presented in Figures 5-7. Figure 5 shows the image and typical electron diffraction of a pristine *IF* nanoparticle. Figure 6 has been obtained from an intercalated sample, which was not exposed to air. Figure 7 was obtained from a sample which was exposed to the ambient atmosphere for one week.

Small wavy-shaped distortions along the *c*-axis can be discerned in the external atomic layers of the fresh sample (Figure 6a, b), while the internal layers remain intact. The electron diffraction pattern shows broadening of the (00*l*) rings, which is indicative of some disorder of the layers after intercalation (Figure 6c).

After exposure to ambient conditions, significant expansion along the *c*-axis with different degrees of swelling was observed for the external layers of the intercalated *IF*-MoS_2 sample (Figures 7a, b). However, the electron diffraction pattern (Figure 7c) shows only one additional ring of the expanded lattice which can be identified as (002)′ with the most frequently observed $c/2 = 8.4$ Å ($\Delta c/2 = 2.13$ Å). These observations gave further support for the intercalation of alkali metal atoms between the MS_2 layers of *IF* nanoparticles and subsequent insertion of water molecules.

EDS/TEM analysis indicates the presence of intercalant atoms (K or Na) in the individual *IF* nanoparticles. However, some nanoparticles did not show any signal of potassium, which indicates that they were not intercalated at all. These results are indicative of an inherent inhomogeneity of the sample, which is in agreement with XRD and EDS analyses. EDS/TEM analysis indicates also an appreciably smaller uptake of the intercalant into particles with a quasi-spherical shape as compared with nanoparticles with polyhedral shape. Most likely, the point defects at the grain boundaries of the nanoparticles with polyhedral shape permit facile intercalation of the dopant. Furthermore, the polyhedral shaped nanoparticles suffer from relatively small elastic strain, characteristic of this structure,[38] which allows an easier metal intercalation into such nanoparticles. The present analysis shows that fullerene-like nanopar-

(38) Srolovitz, D. J.; Safran, S. A.; Homyonfer, M.; Tenne, R. *Phys. Rev. Lett.* **1995**, *74*, 1778.

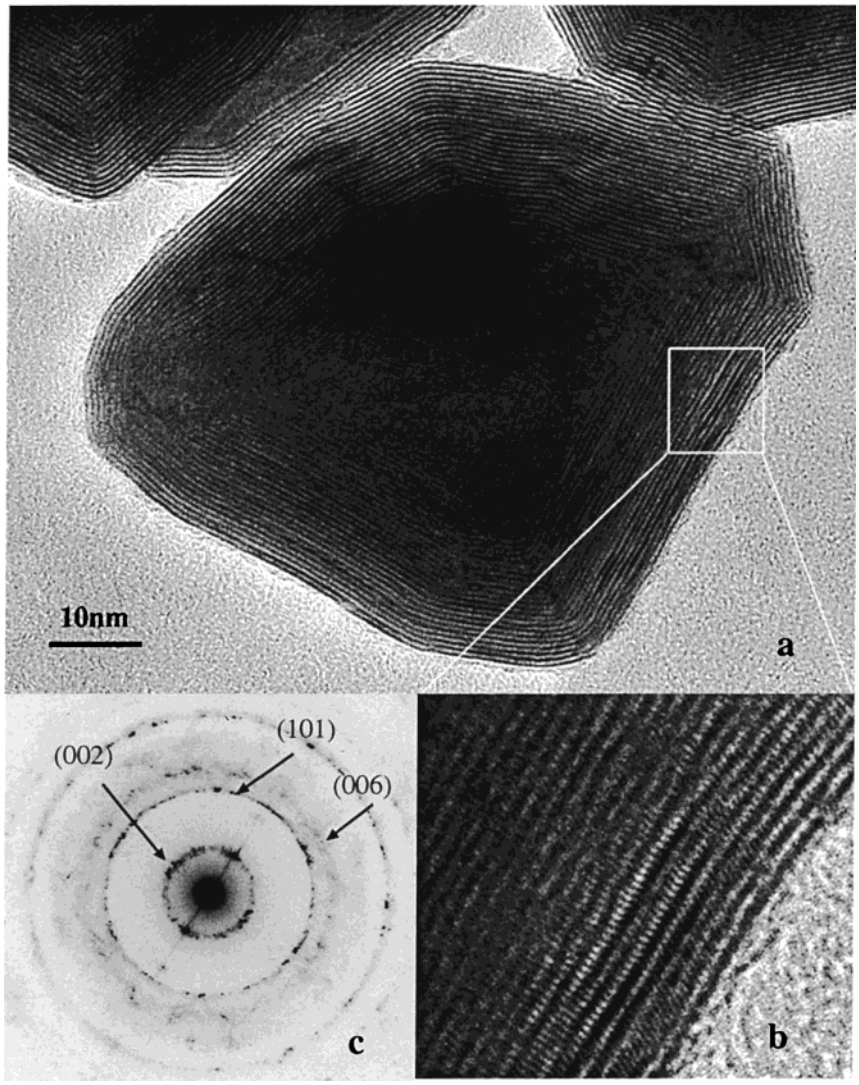

Figure 6. (a) TEM micrograph of the K-intercalated *IF*-MoS_2 nanoparticles (fresh sample); (b) exploded view of the frame; (c) electron diffraction of (a).

ticles of spherical shape and diameter larger than ca. 40 nm can be partially intercalated into the few outermost atomic layers only, while the inner sulfide layers remain intact. Smaller nanoparticles cannot be intercalated at all. This effect is also attributed to the larger elastic strain in smaller nanoparticles.

It appears from the present analysis that there are three kinds of inhomogeneities in the intercalated *IF* samples. First, it is clear that while some of the nanoparticles were intercalated, others remained intact in the process, irrespective of their size and shape. Another source of inhomogeneity stems from the fact that spherical shaped *IF* nanoparticles smaller than ca. 40 nm cannot be intercalated, most likely due to strain effects. Third, in larger nanoparticles the metal atoms did not penetrate to the core, leaving the inner layers of the nested *IF* structure intact, while in the outer layers the guest atoms are ordered with stage 1 arrangement (occupying each interlayer space). The latter two phenomena can be attributed to strain effects, while the reason for the existence of a completely nonintercalated nanophase is not fully clear.

The TEM study of the *IF* nanoparticles, stored in ambient atmosphere for some months, reveals that the slightly intercalated samples return to their pristine form. However, for the heavily intercalated fullerene-like nanoparticles, the deintercalated lattice was quite as perfect as the fresh sample with dislocation disrupting the long-range order. The former may now enable easier reintercalation of alkali atoms into the host *IF* lattice.

4. X-ray Photoelectron Spectroscopy (XPS). XPS measurements were done on fresh samples, which were transferred from the glovebox to the XPS setup without exposure to the atmosphere. Some of the results are summarized in Table 3. A more detailed account of this study will appear elsewhere. First, it was found that the concentration of the intercalated alkali-metal atom is considerably higher in the 2H platelets as compared with the *IF* nanoparticles. These results are consistent with those found by XRD and EDS analyses. The higher concentration of the alkali atom in the 2H platelets is attributed to the existence of 'open' *(hk*0) edges in these particles, which are typically absent from the seamless *IF* nanoparticles.

An interesting support for the intercalated state of the alkaline element within the MS_2 host lattices is provided by the time evolution of the alkali metal signal under elevated (negative) charging conditions. Applying a controlled high flux of electrons from the flood-gun neutralizer,[39] strong electrical fields are

(39) Doron-Mor, I.; Hatzor, A.; Vaskevich, A.; Boom-Moav, T.; Shanzer, A.; Rubinstein, I.; Cohen, H. *Nature* **2000**, *406*, 382.

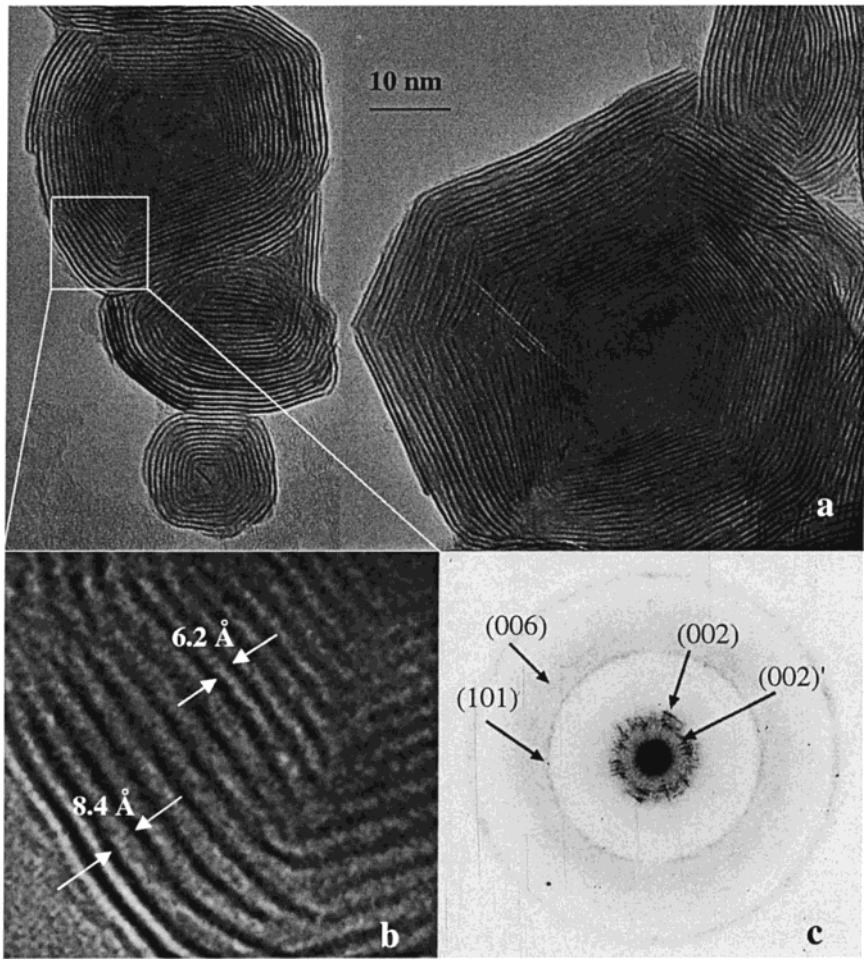

Figure 7. (a) TEM micrograph of the K-intercalated *IF*-MoS_2 nanoparticles after one week exposure to ambient atmosphere; (b) exploded view of the frame and (c) electron diffraction of (a).

Table 3. Summary of the XPS Data

	Alkali metal:Mo(W) atomic ratio			
	+ K		+ Na	
samples	as received	after neutralizer[a] (surface enrichment-%)[b]	as received	after neutralizer[a] (surface enrichment-%)[b]
2H-MoS_2	1:2.5	1:1 (150)	1:0.93[c]	1:0.51 (82)[c]
IF-MoS_2	1:8	1:6 (33)	1:9	1:8 (10)
IF-WS_2	1:17	1:9 (90)	1:13	1:13 (1)

[a] After a 15-h irradiation of the flood-gun on the sample. [b] Increase in the concentration of the alkali metal at the surface induced by irradiation with the flood-gun (deintercalation). [c] These data indicate the presence of Na on the surface of the intercalated material (Na:Mo > 1) as a result of alkali metal excess during the intercalation. However, the increase in the concentration of the alkali metal at the surface induced by strong electric field with the flood-gun (deintercalation) provides strong evidence for the existence of guest atoms inside the crystal matrix.

formed across the particles. A significant surface enrichment of the alkali metal concentration occurs along a typical 5−20 h period, as indicated in Table 3. It is believed that the ionic nature of the alkali metals plays an important role in this type of 'dry electrochemistry'. The positive alkali metal ions diffuse out from the host lattice toward the extra negative charge induced on the surface by the electron beam flux. This out-diffusion process could not be obtained with low bias voltages of the flood-gun. This fact suggests that a critical field is needed for the deintercalation. Furthermore, the efficiency of the deintercalation process varies between the different samples. It is clearly much higher in the 2H matrixes as compared to their *IF* analogues. Also, K is found to outdiffuse from the host lattice much faster than Na.

5. Transport and Magnetic Properties. Transport and magnetic properties measurements gave additional evidence for the successful intercalation process. These measurements were carried out on the partially intercalated materials consisting of a mixture of nonintercated and intercalated phases. The 2H-MS_2 (M = Mo, W) materials are semiconductors[40,41] with a gap between the filled d_{z^2} subband (the top of the valence band) and the conduction band based on the higher-lying $d_{x^2-y^2}$ and d_{xy} orbitals. Upon intercalation an ionization ($K \rightarrow K^+ + e^-$) of the intercalant occurs, resulting in donation of electrons into the lowest empty energy band.

5.1. Magnetic Susceptibility Measurements (MSM). MSM were performed for all four kinds of the materials (2H-MS_2 and *IF*-MS_2 (M = Mo, W)), prior to and after intercalation with both kinds of intercalating atoms (K, Na). However, only the data for K-intercalated *IF*-WS_2 is presented here.

Tungsten and molybdenum disulfides with trigonal prismatic coordination of metal atoms are diamagnetic,[40] which was confirmed by the present measurements (not shown). Magnetic susceptibility of -10^{-7} to -10^{-6} emu/g was obtained for these materials. The original bulk diamagnetism is preserved in the

(40) Wilson, J. A.; Yoffe A. D. *Adv. Phys.* **1969**, *18*, 193.
(41) Friend, R. H.; Yoffe, A. D. *Adv. Phys.* **1987**, *36*, 1.

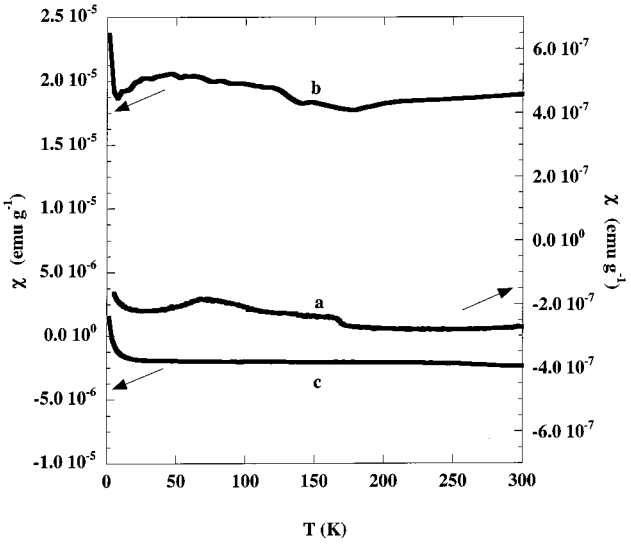

Figure 8. Magnetic susceptibility obtained at 100 Oe (a) for pristine *IF*-WS_2; (b) for K-intercalated *IF*-WS_2; (c) for deintercalated *IF*-WS_2.

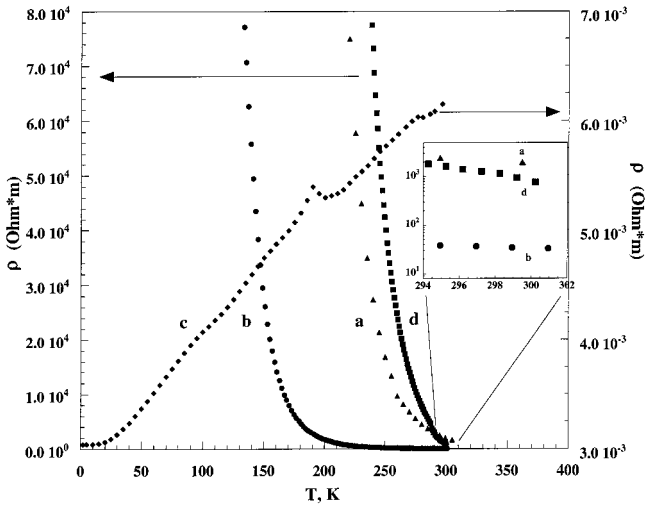

Figure 9. Resistivity versus temperature for (a) pristine 2H−MoS_2, (b) K-intercalated 2H−MoS_2 with 12 at. % of intercalant; (c) K− intercalated 2H−MoS_2 with 18 at. % of intercalant and (d) for deintercalated c-sample.

fullerene-like nanoparticles, but nevertheless two new magnetic transitions are revealed at 60 and 160 K, as shown in Figures 8a. Similar transition occurs at 60 K also for the oxide nanoparticles, which serve as the precursors for the *IF*-MS_2 synthesis. However, single-crystal WO_3 is diamagnetic, while MoO_3 is a very weak paramagnet[42] and they do not exhibit the aforementioned magnetic transitions at 60 and 160 K. Therefore, it is not clear at this point whether these new magnetic transitions (Figure 8a) are indicative of an incomplete conversion of the oxide nanoparticles to the fullerene-like sulfides, or perhaps can be related to a strain induced transitions in the *IF* structure. Moreover, a condensed film of oxygen, which is molecular solid at temperatures up to 54.4 K, is known to exhibit similar transitions.[43] In the present measurements, these transitions can also be amplified by oxygen absorption on the large surface area of the nanoparticles.

A transformation from diamagnetic to paramagnetic behavior occurs for the intercalated samples. Furthermore, most of the samples exhibit temperature independent magnetic behavior, as shown in Figure 8b for K-intercalated *IF*-WS_2. Such temperature independent magnetic susceptibility, i.e., Pauli paramagnetism, characterizes free electrons.[44] Thus, the transformation from diamagnetic to paramagnetic behavior may be attributed to the charge transfer from the intercalated alkali atoms to the unoccupied *d* bands and to the increasing concentration of the free electron in the host lattice. This is consistent with previous reports regarding alkali metal intercalated 2H-MoS_2 and 2H-WS_2 materials,[7,15] as well as hydrazine intercalated TiS_2.[41] The magnetic susceptibility of the other intercalated samples is estimated to be of $10^{-6} - 10^{-5}$ emu/g.

MSM of the intercalated *IF*-WS_2 after storage in the ambient atmosphere for six months reveals that the sample became, once more, diamagnetic (see Figure 8c). These results indicate that deintercalation of the alkali atoms took place. Note, that deintercalated sample has larger negative magnetic moment than the pristine one. This fact indicates that small paramagnetic components exist in the pristine powder, perhaps due to inclusion of some unidentified impurities. During deintercalation, the water of hydration reveals some cleaning effect, taking away not only the intercalated species but also the original impurities. Transport property measurements, which will be discussed below, provide additional evidence for this hypothesis.

5.2. Transport Properties. Figure 9 presents resistivity (ρ) versus temperature measurements for 2H-MoS_2 before and after K-intercalation. The pristine sample shows typical semiconductor characteristics (Figure 9a). Sample with lower concentration of the alkali atom (12%) exhibited semiconductor behavior (Figure 9b) too, however, with a reduced resistivity (see insert to Figure 9) when compared with the pristine sample. The sample containing the highest metal concentration (8−18%), as measured by EDS analysis, exhibited normal metallic behavior (Figure 9c). Prolonged storage of the sample with alkali metal concentration of 8−18% in ambient conditions results in deintercalation and, consequently, in reappearance of semiconductor behavior as shown in the Figure 9d.

Resistivity vs temperature measurements were done for all four kinds of pristine materials before and after intercalation. Metallic behavior was not observed in any other sample. However, the room-temperature resistivity and the apparent activation energy (E_A) were affected by the intercalation as summarized in Table 4. All the materials studied show a one to six orders of magnitude reduction in the room-temperature resistivity and a two- to five-fold decrease in E_A, as a result of the intercalation. The values of E_A were calculated from resistivity versus temperature curves using an Arrhenius equation. In general, higher E_A values were obtained for the fullerene-like nanoparticles in comparison to the bulk 2H phase, in both the pristine and intercalated samples. Surprisingly, the room-temperature resistivity of the deintercalated sample became lower than that of the pristine material, while the activation energy increased significantly, approaching a value of the direct band gap (E_g) for 2H-MoS_2 single crystal, which varies between 1.74 and 2.27 eV depending on the source of the data.[45] This observation correlates with the magnetic measurements, which

(42) *CRC Handbook Chem. Phys*; 69th Edition; CRC Press: Boca Raton, 1988−1989; p E−131 and E−129.
(43) Gregory S. *Phys. Rev. Lett.* **1978**, *40*, 723.
(44) Kittel, C.; *Introduction to Solid State Physics*; John Wiley & Sons: New York, 6th ed., p 396.
(45) Aruchamy, A.; Photoelectrochemistry and Photovoltaics of layered Semiconductors; Kluwer Academic Publishers: Netherlands, p 37.

Table 4. Room Temperature Resistivity and Apparent Activation Energies for Pure and Intercalated 2H−MoS_2 and *IF*-MoS_2.

	Pristine		K-intercalated[a]		Na-intercalated[a]	
sample	E_A (eV)	ρ(Ohm*m) at 300 K	E_A (eV)	ρ(Ohm*m) at 300 K	E_A (eV)	ρ(Ohm*m) at 300 K
2H-MoS_2	0.55	1.5×10^3	0.45 (12 at. %)	3.3×10^1	0.28 (3 at. %)	7.7
			metal (18 at. %)	6×10^{-3}	0.17 (9 at. %)	4.5
			1.86(deintercal.)	8×10^2	0.08 (14 at. %)	0.1
IF-MoS_2	0.62	7×10^3	0.28 (8 at. %)	2.4×10^1	0.20 (10 at. %)	4.1×10^1

[a] Concentration of the intercalated alkali metal is given in the parentheses.

suggested a cleaning effect of the outgoing water molecules in the deintercalated sample.

In the case of Na-intercalated 2H-MoS_2, ρ and E_A were measured for three concentrations of the intercalant (Table 4). The higher the Na at. %, the smaller the resistivity and the activation energy. In the case of K-intercalated 2H-MoS_2, increasing the K concentration resulted in a semiconductor to metal transition as shown in Table 4.

If each intercalated atom would contribute a free electron to the conduction band of the host, metallic behavior would be expected for most, if not all, the intercalated samples. Instead, most intercalated samples preserved their semiconductive behavior. Nevertheless, a relatively mild decrease in the resistivity values and activation energy were observed after intercalation. It is important to emphasize that partial oxidation of the exposed samples could occur during the preparation of the contacts in the ambient atmosphere, which may influence their characteristics. Water insertion during or after the metal intercalation could led to neutralization of part of the free carriers, giving a partial explanation for the lack of metallic behavior in the intercalated samples.

Furthermore, metallic behavior requires an intimate contact between the nanoparticles, which is difficult to accomplish with the present method of pellet preparation. Clarifying this point requires further study.

Conclusions

2H-MS_2 and *IF*-MS_2 (M = Mo, W) powders have been intercalated by exposure to alkali metal (potassium and sodium) vapor at elevated temperatures. The intercalation did not yield a pure phase. Instead, both the bulk (2H) and the nanopowder (*IF*) materials led to mixed intercalated/nonintercalated phases. The elastic strain of the closed folded shells of the fullerene-like nanoparticles is believed to be responsible for the incomplete intercalation of these materials, but there is no explanation for the incomplete intercalation of the 2H-phase.

As was demonstrated by XRD, XPS, and EDS/SEM analyses, the intercalation of 2H platelets was found to be more effective (higher at. %) than that of the fullerene-like nanoparticles.

EDS/TEM analysis of the *IF*-MS_2 phase confirms the presence of intercalant atoms in the individual nanoparticles. The integrity of the intercalated *IF* nanostructures was confirmed by TEM imaging, partial distortions in the outermost layers of the nanoparticles was nonetheless observed. The exposure of the intercalated *IF* nanoparticles to ambient conditions results in a significant expansion along the *c*-axis.

A substantial increase ($\approx 3-5$ Å) in the interplanar spacing of the intercalated phase was observed also by XRD analysis, WAXS and by electron diffraction. No changes in the *a*- and *b*- lattice constants were observed. Intercalation of one to two water molecules per intercalated atom was suggested as a possible explanation for this large expansion of the *c*-axis.

The transport and magnetic properties of the intercalated samples changed significantly under intercalation. Heavily (8−18%) K intercalated 2H-MoS_2 exhibited a semiconductor to metallic transition. A transition from diamagnetic to paramagnetic behavior as well as a decrease in room-temperature resistivity and activation energy values were observed for all the intercalated phases.

Deintercalation of the hydrated alkali atoms and restacking of the MS_2 layers was observed by WAXS, XRD, and TEM analyses in all the samples after prolonged exposure to the atmosphere, which was confirmed by recovering of the pristine host compound properties.

Field-induced deintercalation of the particles was also observed, above a threshold voltage of the flood-gun, by XPS technique.

Reversible intercalation of alkali atoms into the host *IF* lattice was demonstrated in this study. However, it is clear that the loading of the nanoparticles by the present method is rather limited. For any foreseeable application, loading of the nanoparticles with metal atoms would have to be increased. It is clear that the large surface area of the *IF* nanopowder could be advantageous for electrode material, provided it would contain sufficient reactive sites for the intercalation/deintercalation process. However, the inert van der Waals surface of the closed nanoparticles presents a diffusion barrier for the intercalation process. Once the alkali atoms are intercalated into the outer closed layers of the *IF* nanoparticle, their large affinity toward the solvent molecules (water in the present case) leads to the formation of defects in the host lattice and, consequently, to a very rapid intercalation of water molecules between the layers. In the partially ruptured *IF* layers, the process could be easily reversed as indicated by the present experiments. Therefore, it is believed that a few cycles of this kind or perhaps a few cycles of intercalation/deintercalation under electrochemical control would make this phase ideally suitable for reversible alkali metal intercalation. The ramifications of this process can be of substantial importance, e.g. to the battery industry.

Acknowledgment. We are grateful to Dr. R. Rosentsveig and A. Margolin for assistance with the synthesis of the *IF*-MoS_2 and *IF*-WS_2 materials; to Dr. C. Lévy-Clément, CNRS-Thiais, Dr. I. B. Zubavichus, Nesmeyanov Institute of Organoelement Compounds, Moscow and Prof. S. Shilstein, Weizmann Institute of Science for enlightening discussions; to Dr. Y. Rosenberg, Tel-Aviv University for assistance in XRD measurements. This work was supported by the Minerva Foudation (Munich) and Alfried Krupp von Bohlen und Halbach Steiftung.

JA012060Q